NUCL SCI TECH (2021) 32:93
https://doi.org/10.1007/s41365-021-00930-x

Evaluation of the passivation effect and the first-principles calculation on surface termination of germanium detector

Sha-Sha Lv[1] · Yuan-Yuan Liu[1] · Wei-You Tang[2] · Li He[3] · Xiu-Xia Li[3] · Jian-Ping Cheng[1]

Received: 24 May 2021 / Revised: 15 July 2021 / Accepted: 16 July 2021 / Published online: 6 September 2021

Abstract The point-contact high-purity germanium detector (HPGe) has the advantages of low background, low energy threshold, and high energy resolution and can be applied in the detection of rare-event physics. However, the performance of HPGe must be further improved to achieve superior energy resolution, low noise, and long-term reliability. In this study, we combine computational simulations and experimental comparisons to deeply understand the passivation mechanism of Ge. The surface passivation effect is calculated and inferred from the band structure and density of interface states, and further confirmed by the minority carrier lifetime. The first-principles method based on the density functional theory was adopted to systematically study the lattice structure, band structure, and density of state (DOS) of four different systems: Ge–H, Ge–Ge-NH_2, Ge-OH, and Ge-SiO_x. The electronic characteristics of the Ge (100) unit cell with different passivation groups and Si/O atomic ratios were compared. This shows that H, N, and O atoms can effectively reduce the surface DOS of the Ge atoms. The passivation effect of the SiO_x group varied with increasing O atoms and Si/O atomic ratios. Experimentally, SiO and SiO_2 passivation films were fabricated by electron beam evaporation on a Ge substrate, and the valence state of Si and resistivity was measured to characterize the film. The minority carrier lifetime of Ge-SiO_2 is 21.3 μs, which is approximately quadruple that of Ge-SiO. The passivation effect and mechanism are discussed in terms of hopping conduction and surface defect density. This study builds a relationship between the passivation effect and different termination groups, and provides technical support for the potential passivation layer, which can be applied in Ge detectors with ultralow energy thresholds and especially in HPGe for rare-event physics detection experiments in future.

Keywords Germanium detector · Passivation · Surface termination

1 Introduction

Bulk germanium (Ge) is an indirect band-gap semiconductor with a band gap of 0.67 eV at room temperature. The high carrier mobilities of electrons and holes at room temperature are 3900 cm^2/Vs and 1900 cm^2/Vs, which are approximately 2.6 and 4.2 times that of silicon [1, 2], respectively. High-purity Ge detectors (HPGe) have the advantages of high energy resolution, high detection efficiency, and strong stability for the detection of particles, especially X-rays and γ-rays [3, 4]. Point-contact HPGe detectors have the advantages of low background and low energy threshold; thus, they can be applied in the detection

This work was supported by the National Natural Science Foundation of China Youth Fund (No. 12005017)

✉ Sha-Sha Lv
lvss@bnu.edu.cn

✉ Yuan-Yuan Liu
yyliu@bnu.edu.cn

[1] Key Laboratory of Beam Technology of Ministry of Education, College of Nuclear Science and Technology, Beijing Normal University, Beijing 100875, China

[2] Department of Engineering Physics, Tsinghua University, Beijing 100084, China

[3] Joint Research Center, Nuctech Company Limited, Beijing 100084, China

of rare-event physics (e.g., dark matter direct detection and neutrinoless double beta decay).

Many international experimental groups, including China's dark matter experiment (CDEX), the germanium detector array (GERDA), cryogenic dark matter search (CDMS), coherent germanium neutrino technology (CoGeNT), Majorana, and EDELWEISS, have used HPGe detection systems to carry out relevant detection experiments [1–14]. The main objective of these experiments was to increase the sensitivity by enlarging the scale of the detector array, improving the performance of energy resolution, linearity, and stability, and suppressing background and electronic noise.

The direct detection of dark matter at a low background is leading the frontiers of physical research. Currently, the search parameter space and annual modulation effect of dark matter are experiencing fierce competition [6–8]. To improve the detection sensitivity of dark matter in a low-mass regime, the energy threshold and background environment need to be further reduced [9]. Point-contact and broad-energy Ge (PCGe and BEGe) detectors are highlighted in these experiments and related applications for their balance of high efficiency, high energy resolution, and low input capacitance (thus low serial noise). One desirable solution for future ton-scale HPGe-based experiments is to directly operate the bare detector array with low-mass electronics in a cryogenic liquid [15, 16].

Direct operation of a bare HPGe detector in a cryogenic liquid is desirable for rare-event physics experiments because of its potential to realize ultralow background and ultralow noise [12–14]. However, the interface problem of Ge is an important factor that limits the performance of HPGe [10–12]. First, Ge cannot form a stable passivation layer spontaneously like silicon dioxide on silicon, and the natural oxide of Ge is unstable and readily decomposes, introducing a high density of defect states at the interface between Ge and other materials. The natural oxide of Ge decomposes into several low-valent oxides of Ge_xO_y. Among them, GeO_2 has high water solubility, poor interface characteristics, and instability. Second, processing and treatment introduce dangling bonds on the Ge crystal, which reduces its chemical stability and produces high-density defect states at the interface. Finally, the surface state results in a decrease in carrier mobility and a higher leakage current, leading to disadvantages in realizing the stability and promotion of the device performance. All of these limitations prevent the realization of low power consumption and the stability of Ge devices.

The energy threshold of the detectors is directly related to the electronic noise, further requiring low leakage currents [17]. The leakage current includes the bulk leakage current (minor carrier diffusion current, generation-recombination current, and tunneling current) and surface leakage current. The probability of generation–recombination is negligible at 77 K, and the minor carrier diffusion current and tunneling current can be controlled very well when the detector contacts are well made. Thus, the bulk leakage current is small, and the surface leakage current becomes the main influential factor.

The main factors affecting the surface leakage current of HPGe are as follows: (1) Contaminants and humidity on the crystal surface can change the surface state of Ge. This is because carriers are generated or recombined through the interface state at recombination centers, resulting in a high interface state density. (2) When the surface states are introduced into the forbidden band, defective energy levels can result in Fermi-level pinning and band bending. The relative position of the Fermi level determines the potential difference and controls the surface recombination rate, surface leakage current, and noise [18]. (3) The interfacial electric field and charge collection of the surface passivation layer lead to an increase in leakage current [19]. Therefore, surface dangling bonds directly affect the band structure and density of states (DOS) of Ge.

The leakage current, energy threshold, and other characteristics of HPGe with surface passivation deserve further investigation [20, 21]. From an atomic-scale analysis, the interaction between the outermost Ge atoms and surface termination functional groups is different in strength. The theoretical first-principles calculations of Ge unit cells mainly focus on the band structure and electronic properties of different groups on the diameter, crystal orientation, and doping atoms of unit cells. Merid et al. found that the highest occupied orbitals and the lowest occupied orbitals of unterminated Ge occur more locally with surface states [22]. The unsaturated dangling bonds on the surface of the Ge unit cell introduce surface states and increase the unit cell conductance [21]. The passivation can reduce the leakage current by decreasing the interface state density.

In traditional HPGe detector processing technology, hydrogen ions are typically used to passivate the surface dangling bonds of Ge and reduce its surface interface state. HF, NH_4F, HCl, and HBr can remove surface oxides and provide H-terminated surfaces [22, 23]. However, the stability of hydrogen passivation is poor, and the passivation effect of H is poor with insufficient passivation, which affects the stability of the leakage current. Hydrogen passivation can be used as a pretreatment of the surface passivation layer to obtain a clean surface. A passivation layer with high quality and low interface state density is processed on the HPGe detector by evaporation and sputtering, which can effectively eliminate the influence of surface recombination. The Ge-passivation treatment methods include [21–26] the plasma surface treatment of NH_3 and PH_3, SiO_x, GeO_x, GeN_x, GeO_xN_y, Al_2O_3, AlN, etc. The flexibility of the Si–O-Si bond in SiO_x saturates most of the

chemical bonds at the interface, so SiO_x has excellent electrical and chemical passivation properties. Because of the high reactivity of Si, the valence state of Si in the SiO_x film is between 0 and 4, and the x value of the oxygen content in the SiO_x film is between 0 and 2.

The SiO_x passivation layer not only reduces the interface state density but also achieves good passivation results through a built-in electric field formed by the fixed charge in the oxide layer. Therefore, the SiO_x/Ge interface with an appropriate atomic ratio has a lower interface state density and fixed charge density, and it can match the energy band structure and low interface potential. All of these characteristics of SiO_x achieve good control of the surface leakage current. At the same time, the low dielectric constant of SiO_x can reduce the generation of oxide charges and surface energy bands.

It is known that HPGe passivation technology mainly involves depositing high-quality SiO_x films as the passivation layer [22]. The SiO_x passivation layer can reduce the DOS and achieve good passivation with an internal electric field formed by the fixed charge of the oxide layers. Furthermore, owing to the small dielectric constant of SiO_x, the generation of surface energy states and oxide charges after radiation can be reduced. Because of the high reactivity of Si, the valence state of SiO_x is distributed between 0 and 4. Because of the flexibility of Si–O-Si bonds in SiO_x, most of the chemical bonds at the interface remain saturated, and the SiO_x/Ge interface with a suitable atomic ratio has a lower interface state density, fixed charge density, matched band structure, and small interface potential difference. This can achieve good control of the surface leakage current with excellent electrical and chemical passivation properties.

To further reduce the energy threshold of HPGe, it is important to lead the international competition toward dark matter detection [27, 28]. Surface passivation has been the key technology for realizing detectors with ultralow energy thresholds [29–32]. In this study, we combine computational simulations with experimental comparisons to promote the passivation effect of Ge. First-principles simulations are used to modify different groups of dangling bonds on the Ge surface. First, the energy band structure, band-gap width, and DOS of passivation groups -H, -N, -O, and -SiO_x on the Ge surface are theoretically calculated. The interface state density and potential of the passivation layers with different atomic ratios are accurately analyzed. A comparison between the DOS of different groups and atomic ratio termination is precisely analyzed to find a relatively suitable surface passivation layer. In addition, the related mechanism of stable surface state formation is deeply understood. Then, the preparation conditions, minority carrier lifetime, and passivation effect of SiO and SiO_2 passivation layers on the Ge surface of a single crystal by electron beam evaporation are systematically studied to determine the appropriate passivation process.

2 Calculation and experimental methods

2.1 Parameter settings of Ge

The space group of the Ge cubic crystal system is Fd-3 m with an electron arrangement of $1s^2 2s^2 2p^6 3s^2 3p^6 3d^{10} 4s^2 4p^2$. The Ge atoms occupy face-centered cubic nodes and four complementary adjacent tetrahedral gap positions in the unit cell. The energy–momentum (E-k) relationship of the band structure is obtained by solving the single-electron approximate Schrödinger equation using the Materials Studio CASTEP module. The generalized gradient approximation is used as an independent exchange–correlation function with gauge conservation pseudopotentials. A cut-off energy of 440 eV, k points of $4 \times 4 \times 4$, and an energy convergence accuracy of 1.0×10^{-5} eV/atom are used in the simulation. The optimized lattice constant is 5.59 Å after relaxation, which is very close to the experimental value of 5.65 Å [17]. The indirect band gap is 0.667 eV with the valence band maximum (VBM) at the origin of the k-space at point G, and the conduction band minimum (CBM) is at the 111-direction boundary of the k-space at point L. These results are consistent with those of previous studies [24]. For the part of the valence band (− 5 eV to 0) of the Ge single crystal, the 4p orbital electrons are the main contributors. In the conduction band field, the 4p orbital state density is slightly higher than that of the 4 s orbital.

2.2 Model construction and parameter settings of surface termination on Ge

In the visualizer module of the MS software, the Ge crystal was cut to obtain a super cell structure with a specific growth direction. To avoid the mutual influence of the periodic unit cells, a vacuum layer of 10 Å was added around, thus obtaining a cross-sectional period of (d + 10 Å) one-dimensional Ge supercell, where d represents the diameter of the unpassivated Ge unit cell. Then, a Ge-passivation atom model was constructed by adding functional groups, and the energy band structure and DOS were further calculated after optimizing the structure by relaxation. Based on the unpassivated Ge cell structure in the (100) direction, a saturated passivation layer structure of -H, -NH_2, and -OH was constructed. There are 16 Ge atoms and 16 passivation groups (H, NH_2, and OH) in three types of supercells to form bonds with them, and two or one henry atoms are added to each N atom and O atom to form a stable electronic structure, respectively.

Similarly, four types of passivation layer structures with different numbers of silicon and oxygen atoms were constructed. Refer to the calculation method for the band structure of the Ge unit cell with saturated hydrogen passivation. The local density approximation, generalized gradient approximation, and gauge conservation pseudopotentials were used to calculate the energy band structure. The cut-off energy was 650 eV with k points set to $4 \times 1 \times 1$, and the energy convergence accuracy was 1.0×10^{-5} eV/atom.

2.3 Passivation film preparation and effect evaluation

The deposition substrate was an inner-circle cut Ge (100) single crystal with a diameter of 50 mm, and its resistivity was approximately 5–40 Ω·cm. The organic impurities on the surface of the Ge substrate were removed using ethanol, acetone, and deionized water ultrasonic cleaner for 15 min before deposition. The Ge substrate was then blow-dried with high-purity N_2. ATS-500-type electron beam evaporation coating equipment was used, and the targets of SiO and SiO_2 had a purity of 99.99%. The chamber was vacuumed to 5×10^{-6} mTorr using a molecular pump before the coating process.

The minority carrier lifetime is the average survival time of minority carriers from generation to recombination after electron–hole pair separation in semiconductor materials, generally in microseconds. Passivation is typically used to reduce the recombination rate of the sample surface and enhance the minority carrier lifetime. Microwave photoconductivity attenuation (μ-PCD) was used to measure the minority carrier lifetime. When the pulsed light source irradiates the sample surface, the conductivity of the sample changes, further affecting the reflected microwave energy. Therefore, the lifetime of nonequilibrium carriers is reflected by changes in conductivity. At a low injection level and certain frequency, the difference between the emitted and reflected microwave signals is proportional to the unbalanced carrier concentration. The minority carrier lifetime was obtained by fitting an exponential decay signal. The minority carrier lifetime measured in the μ-PCD system τ_{Meas} is the composite and comprehensive embodiment lifetime of the bulk and surface. However, the reflectivity of a microwave with a wavelength of 910 nm needs to be decreased; this can be deduced from the sample reflection spectrum. The minority carrier lifetimes of SiO and SiO_2 films with a thickness of ~ 200 nm were measured to evaluate the surface conditions (Fig. 1).

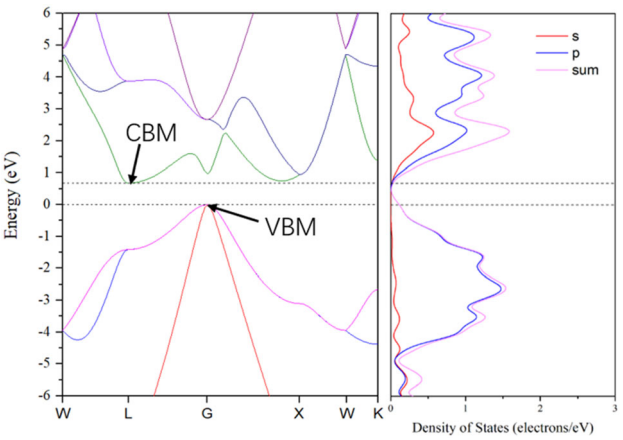

Fig. 1 (Color online) Calculated band structure and DOS for Ge crystal in (100) direction

3 Results & discussions

The lattice structure, electronic energy band structure, and state density information of the -H,-NH_2, -OH, and -SiO_x passivation systems of the Ge surface were studied. The modifications of the energy band structure of the -H passivation and other passivating groups were compared.

3.1 Band structure of Ge termination (-H, -NH_2, and -OH)

The constructed Ge supercell saturated with -H, -NH_2, and -OH and their corresponding band structures are shown in Fig. 2. After structural optimization, the relaxation structures of the Ge supercell passivated by NH_2 and H are similar. The Ge–Ge bond length of surface layer is about 0.01 Å shorter than that of the center. In the system of -OH termination, the Ge–Ge bond length at the surface is 0.01 Å longer than the central Ge–Ge bond. The Ge–H, Ge-NH_2, and Ge-OH termination band gaps are 3.43, 2.68, and 2.46 eV, respectively. Compared with the Ge–H system, the bandwidth of Ge-NH_2 passivation is decreased, and Ge-OH has the shortest bandwidth. The band structures of H- and NH_2-passivated Ge atoms with direct band gaps are similar, and the CBM and VBM are both at the origin of the G point. The Ge-OH system has an indirect band gap, and its CBM is at point G as well. However, the VBM is moved to a position between the Q and Z points in k-space.

3.2 DOS of Ge termination (-H, -NH_2, and -OH)

DOSs with three different termination systems are shown in Fig. 3. At the CBM and Fermi levels, the Ge-NH_2 system has the highest DOS, and the DOS of Ge-OH is lower than that of H termination. It is inferred that Ge-OH

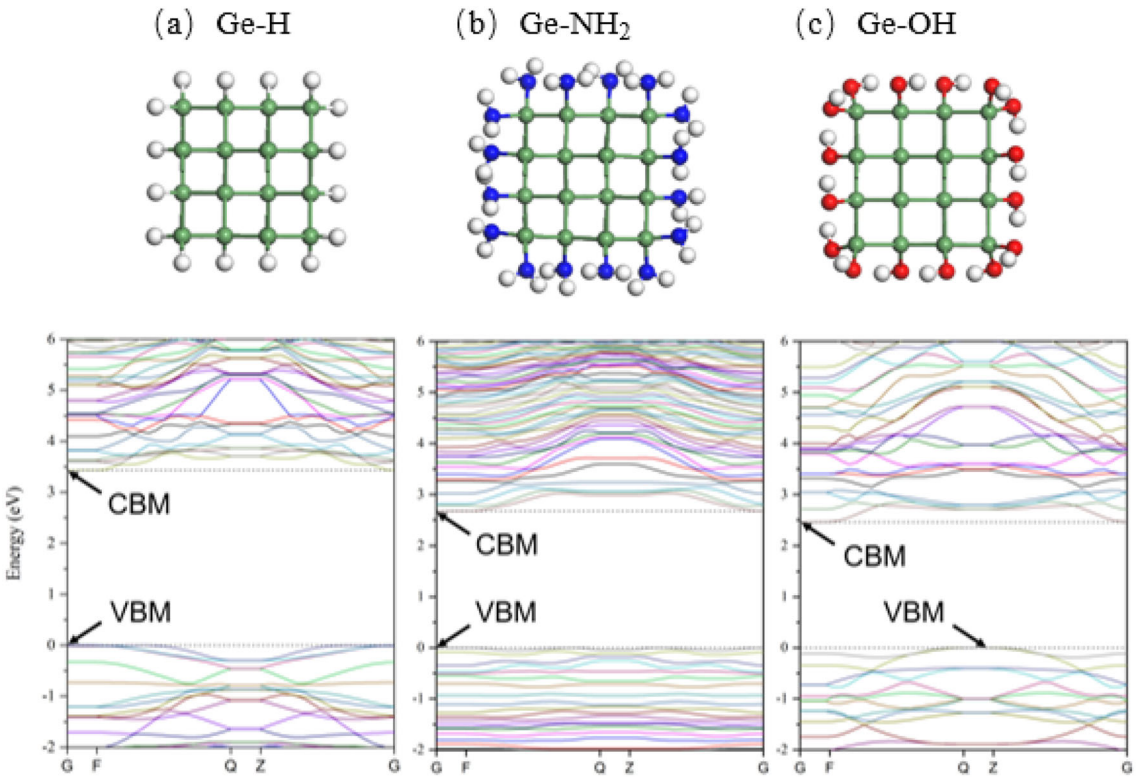

Fig. 2 (Color online) Cross section and corresponding band structures of **a** Ge–H, **b** Ge-NH_2, and **c** Ge-OH termination

could have a better passivation effect than Ge–H and Ge-NH_2 owing to the DOS reduction and the band edge characteristics. Comparing the calculation results of Legesse et al. using the GGA method [25], it was found that the NH_2 and OH terminations both have a reduced band gap compared to the Ge–H supercell. Owing to the strong electronegativity of the terminated atoms, the electron cloud is rearranged, thereby changing the energy eigenvalues at different k vectors, and the electronic state distribution at the edge of the energy band is changed.

Generally, H is the most common passivation atom in Ge nanomodels owing to its surface passivation. In addition, all theoretical calculations on Ge termination were performed on the basis of H atoms. H passivation can be easily obtained by treating the Ge surface with an HF aqueous solution [26]. Dass used an sp^3 tight-binding model to explore the electronic properties of H-terminated Ge cells and found that H saturation causes the band structure to change to a direct band gap. In addition, the bandwidth increases compared to the unterminated system with a highest value of 3.66 eV in the (100) direction [22].

To further analyze the contribution of each orbital to the band structure, the partial DOSs for different termination groups are shown in Fig. 3. Near the bottom of the CBM (2–6 eV), the s- and p-orbitals of Ge–H and Ge-NH_2 make the same contribution, while the DOS of the s-orbital of Ge-OH is significantly lower than that of the p-orbital. The VBM is mainly contributed by p-orbital electrons, and the DOS of the Ge-OH structure changes significantly in the valence band compared to other systems, with the lowest DOS of the s-orbital near the Fermi level.

Comparing the DOSs of different elements in the Ge-NH_2, the H atoms in the NH_2 group contribute to a higher s-orbital DOS in the conduction band, and the p-orbitals of N atoms have a higher DOS near the Fermi level. In the Ge-OH system, the interaction of O and Ge atoms causes the DOS peak of the p-orbital to remain. The p-orbital DOS of O atoms at the VBM was significantly lower than that of the N atoms. Researchers calculated the influence of other passivation groups on the electronic properties of the Ge unit cell. The movement of CBM led to a decrease in the bandwidth, and at the same time, it was transformed into an indirect band-gap structure [28]. In addition, Carturan et al. explored the influence of B and P atom doping on the electronic characteristics and band structure of Ge–H cells [26]. The calculation results showed that n-type and p-type doping produced similar responses to their band structures [30].

Figure 4 shows the partial DOS of Ge atoms and H atoms at different positions to further analyze their influence. The side H atoms are bonded to the outermost Ge atom on the side. Near the VBM (− 4 eV–0), the DOS peak of the p-orbital of the Ge atom at the center is closer to the Fermi level, while that of the corner appears at −

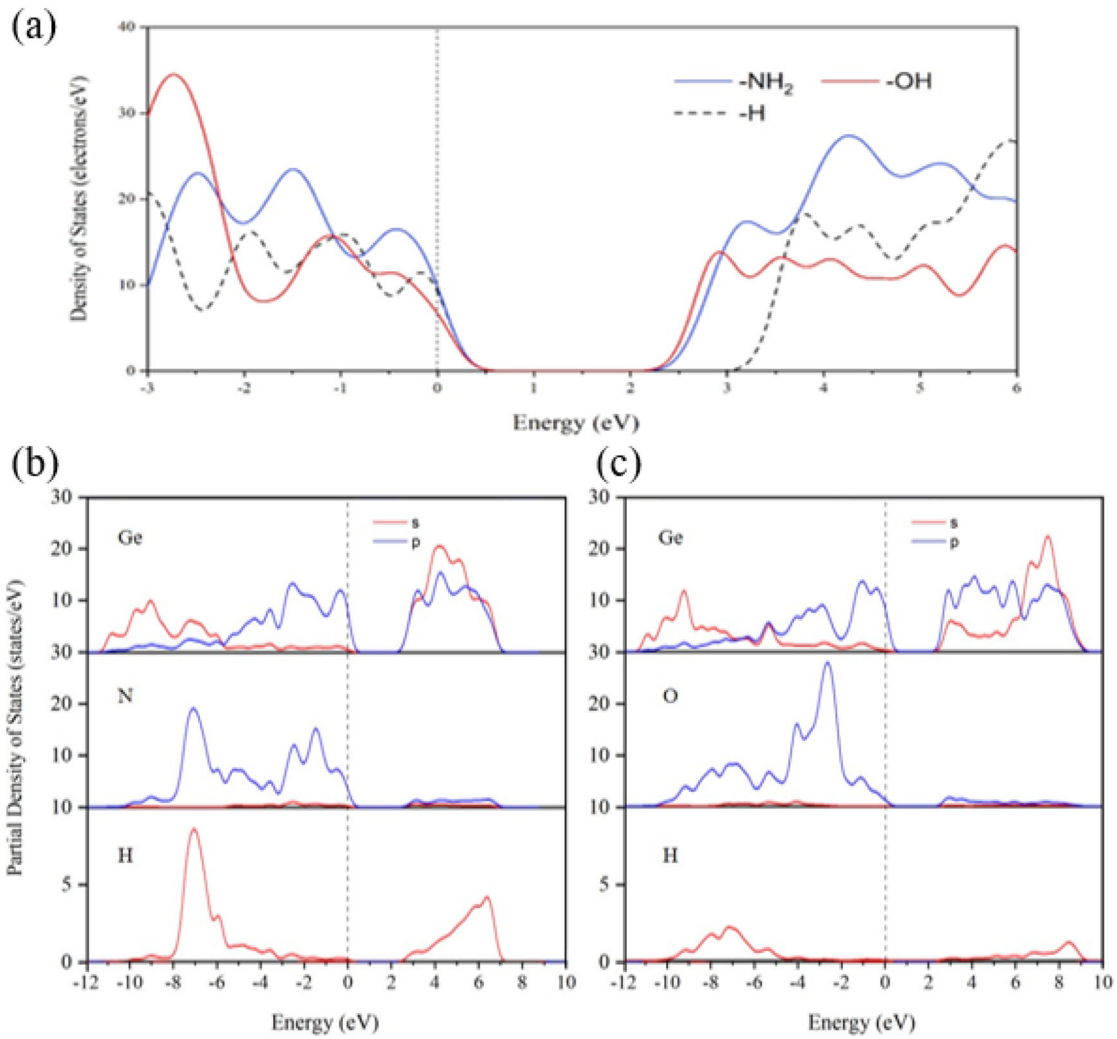

Fig. 3 (Color online) **a** Total DOS of Ge–H, Ge -NH_2, and Ge-OH. **b** Partial DOS of Ge-NH_2. **c** Partial DOS of Ge-OH

3.5. The DOS peak value of the *s*-orbital of the H and Ge atoms appears at the same position, which indicates that the s-orbitals of H atoms interact with the *p*-orbitals of the outermost Ge atoms, thus reducing the DOS near the Fermi level. The DOS of Ge atoms in the middle also proves this interaction, but the side Ge atom has only one dangling bond to form a bond with the H atom, making it not as obvious as the corner Ge atom.

The DOS near the Fermi level is mainly contributed by the 4*p* orbital electron of Ge at the VBM. The termination of H atoms reduces the DOS of the surface Ge atoms compared to the central Ge atomic band, which explains the passivation effect of H on the Ge surface. The Ge-NH_2 passivation has a direct energy band, while Ge-OH passsivation changes to an indirect one, and compared with the passivation of Ge–H, their band gap decreases by 0.75 eV and 0.97 eV, respectively. The passivation effect of Ge-OH is slightly better than that of Ge–H and Ge-NH_2 in reducing the DOSs at the band edges.

3.3 Band structure of -SiO_x termination

The understanding of the SiO_x structure is based on two classical structural models: the random bonding (RB) model and random mixture (RM) model. The RB model indicates that the structure of SiO_x is a single phase consisting of Si–Si bonds and Si–O bonds, which are distributed continuously and randomly throughout the entire network. The RM model indicates that it has a two-phase structure consisting of a mixture of Si and SiO_2 in a very small category.

To clarify the interaction between the Ge and SiO_x groups, it is necessary to consider the termination of different Si/O ratios and their corresponding band structures. The green, yellow, red, and white balls represent the Ge,

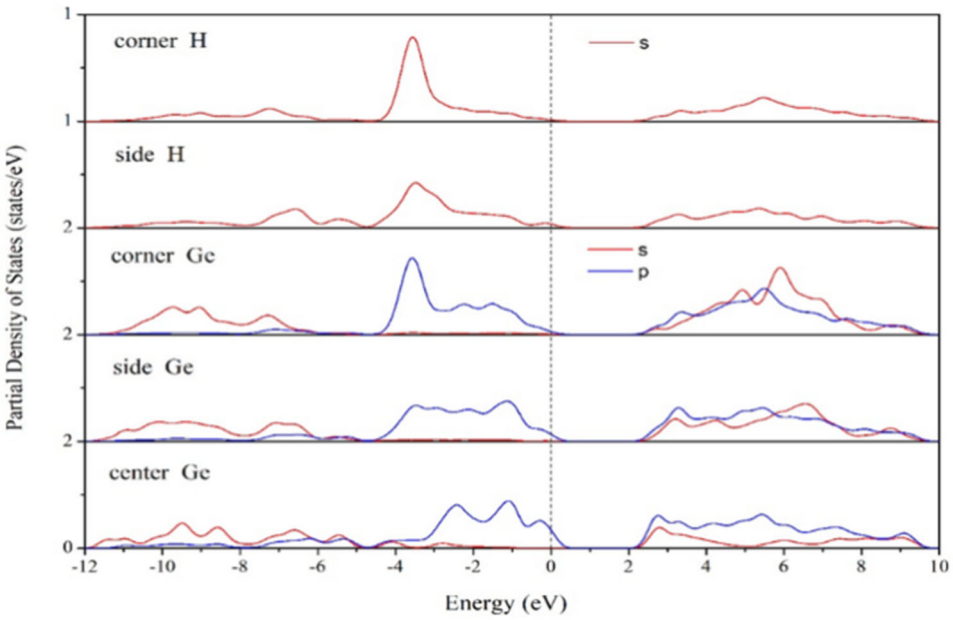

Fig. 4 Partial DOS of Ge–H system

Si, O, and H atoms in the structure, respectively. The energy band of Ge-SiO_x passivation is shown in Fig. 5. After structure optimization, the relaxed structure and band gap of the Ge-SiO_x passivation are related to the atomic ratio. Ge-SiO and Ge-Si_2O_2 systems have similar central symmetry structures, of which the Ge–Ge bond length at the surface is approximately 0.01–0.02 Å shorter than that of the central Ge atom. For Ge-SiO_2 and Ge-Si_2O_3, the Ge–Ge bond length is longer (0.03–0.04 Å) than that of the central Ge atom.

The structure and energy band structures of Ge-SiO_x and Ge–H are listed in Table 1. It can be seen that Ge-SiO_x passivation has an indirect energy band with different degrees of reduction compared with the -H band gap. This

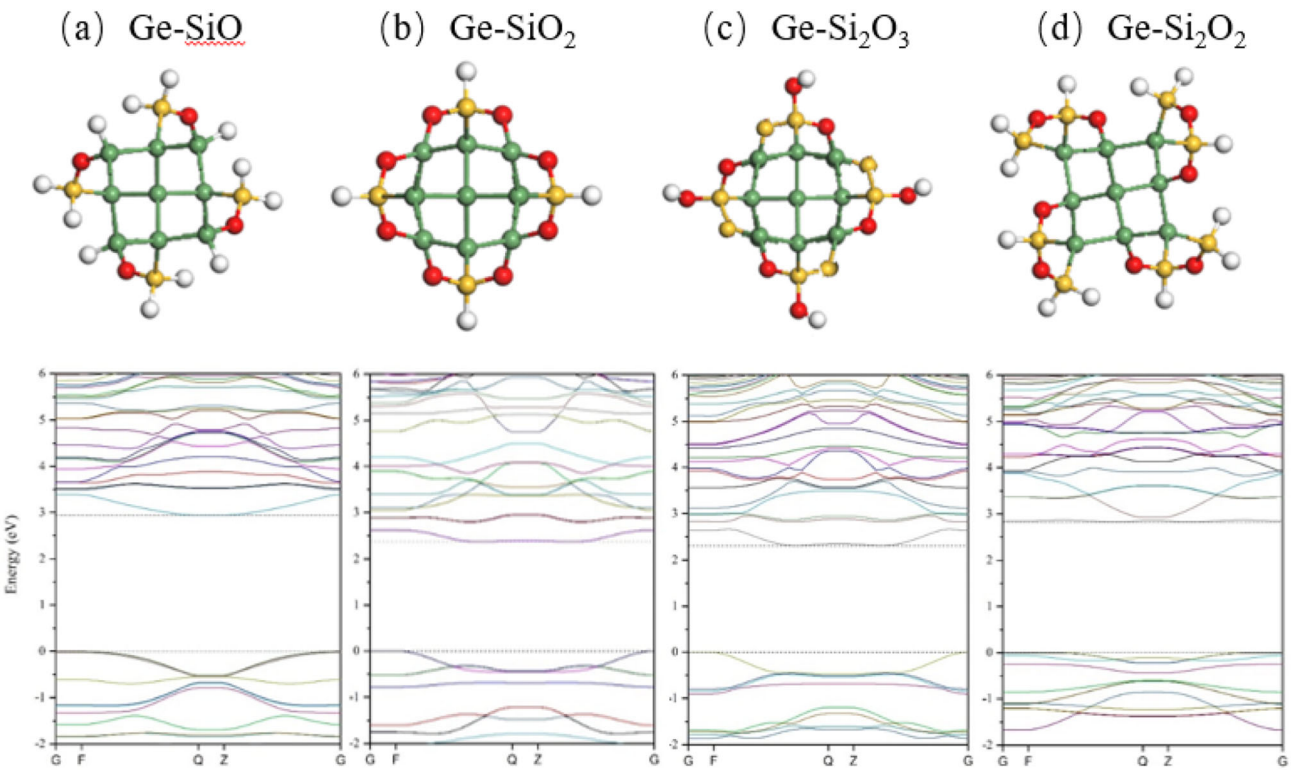

Fig. 5 (Color online) Structural cross-sectional views and corresponding band structures of **a** Ge-SiO, **b** Ge-SiO_2, **c** Ge-Si_2O_3, and **d** Ge-Si_2O_2

Table 1 Ge-SiOx and Ge–H passivation supercell structure and energy band

Direction	Passivation group	Si atom number	O atom number	H atom number	E_g (eV)	Band-gap type
100	-SiO	4	4	12	2.94	Indirect
	$-SiO_2$	4	8	4	2.36	Indirect
	$-Si_2O_3$	8	12	4	2.39	Indirect
	$-Si_2O_2$	8	8	12	2.82	Indirect
100	-H	–	–	12	4.21	Direct

means that the indirect band gap of the Ge-SiO_x system is smaller than that of the Ge–H termination. The VBM is at the origin point G of *k*-space, and the CBM is mainly related to the termination structure. The bandwidth of Ge-SiO_2 passivation is the smallest and is reduced by 1.9 eV compared to the Ge–H system. The Ge-SiO and Ge-Si_2O_2 band structures with more H atoms are discontinuous and have larger bandwidths than the other two.

3.4 DOS of -SiO_x termination

To further analyze the contribution of each orbital to the band structure, the DOS of Ge-SiO_x is shown in Fig. 6. Compared to the Ge–H system, the DOS has different degrees of reduction in the vicinity of the Fermi level, except for the Ge-Si_2O_2 system. Near the CBM (2–6 eV), the contributions of the *s*-orbital and *p*-orbital of Ge–H are basically the same, while the DOS of the *s*-orbital of Ge-SiO_x is significantly lower than that of the *p*-orbital. For the VBM, the peaks of the *s* and *p*-orbitals move away from the Fermi level, of which the Ge-SiO_2 system moves farthest, and its DOS near the Fermi level is the lowest.

For Ge-SiO and Ge-SiO_2, the DOS at the Fermi level is reduced, and their peak shifts to the left, indicating lower surface states. As the ratio of oxygen to silicon increases, the DOS near the Fermi level gradually decreases, and Ge-SiO_2 is the lowest. The DOS peak of Ge-SiO_2 is almost reduced to half that of Ge–H, indicating the best passivation effect. The DOS of Ge atoms is much higher than that of O atoms at the Fermi energy level because the electronegative O atom gains electrons from the Ge atom, which makes the passivation effect better than that of H atoms. Nevertheless, more passivation atoms and passivation layer structures (such as organic groups) can be selected and constructed, providing a better understanding of the chemical bonds between Ge and passivated atoms, as well as the electronic properties of Ge and different surface-passivated atoms.

3.5 Minority carrier lifetime of passivation film

The matching passivation layer of Ge can reduce the surface contaminants and dangling bonds. Covalent bonds between the passivated atoms and the outermost Ge can be formed, and the electronic state distribution at the edge of the energy band can be changed to optimize the energy band structure and reduce the interface state density [31, 32]. Stable and insulating SiO and SiO_2 films were deposited by electron beam evaporation at room temperature. Deposition at room temperature can prevent the diffusion of the passivation film into the Ge substrate, and a higher sputtering pressure reduces the fixed positive charge.

The minority carrier lifetime and electrical resistivity of the SiO and SiO_2 passivation films were measured, as shown in Fig. 7a. Resistivity is an important index that reflects the electrical properties of the passivation films. The four-probe method was used to test the resistivity of the SiO and SiO_2 films. When the constant current source supplies a fixed current to the two probes outside, the voltage drop of the two probes inside is measured by a voltmeter. The square resistance of the sample can be read directly, and the film resistivity can be obtained by multiplying the thickness of the film. The square resistance of bare Ge substrate, SiO, and SiO_2 with a thickness of $\sim$ 200 nm is 0.26 Ω, 249 Ω, and 550 Ω. The film resistivity of SiO_2 (0.011 Ω· cm) is more than twice that of SiO (0.005 Ω· cm).

The electronegativity difference between Si and O is 1.7. The bond angle of the Si–O-Si bond with strong polarity can change in a range of 100° to 170°, and the rotation flexibility of Si–O-Si bonds makes most of the chemical bonds at the saturated interface [33]. In particular, oxygen acts as a bridge in the Si–O-Si bond. The interface between Ge and silicon oxide is a disordered system with dielectric properties. For the amorphous passivation film of an irregular network, the band gap is occupied by a large number of defect states. The frequent scattering and trapping of silicon oxide substantially reduces the charge movement compared to the crystalline mobility. The charge carriers that would normally be forbidden to move

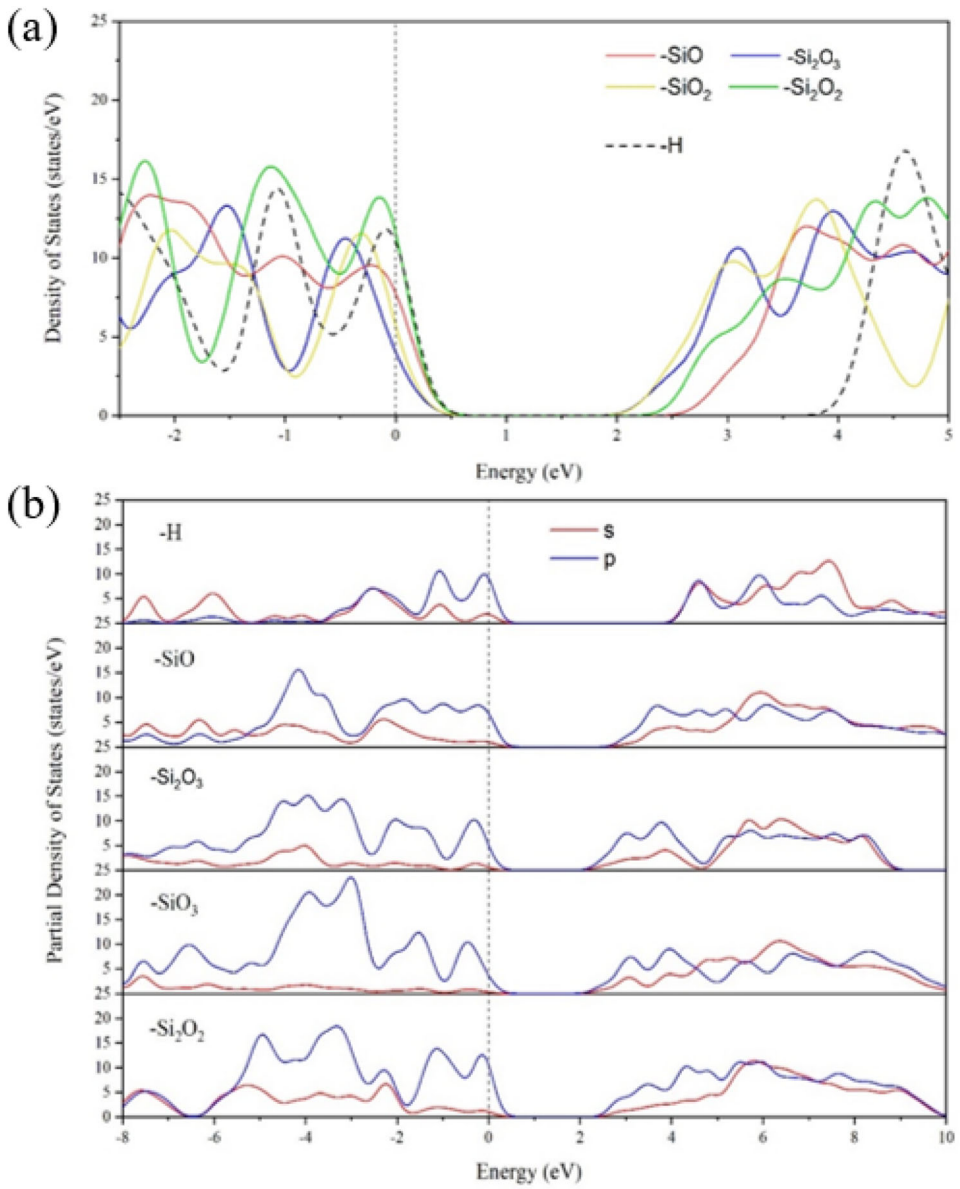

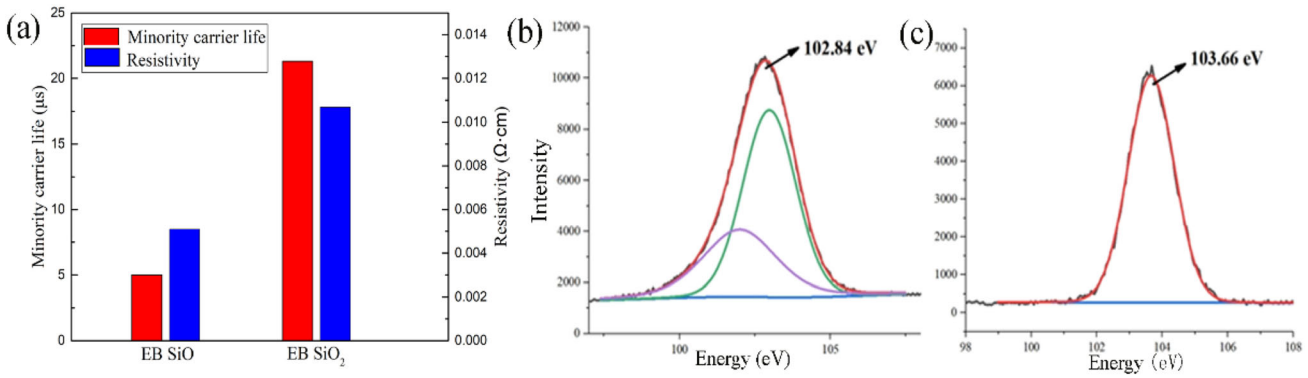

Fig. 6 (Color online) **a** Total and **b** partial DOS of Ge–H and Ge-SiO_x

Fig.7 (Color online) **a** Minority carrier lifetime of SiO and SiO_2 passivation film on Ge by electron beam evaporation, and XPS spectra of **b** SiO and **c** SiO_2 passivation film

in the gap region have a significant number of defect states. They can move from defects to defects in a process called phonon-assisted hopping, allowing for significant conduction near the Fermi level in the gap region. Silicon oxide contains acceptor- and donor-type localized states with considerable densities. The deep donor-type localized states are above the Fermi level, and the deep donor-type localized states are below the Fermi level. Therefore, it was found that the resistivity, Si–O bond, and band gap increased with oxygen content.

The composition and chemistry of the films were characterized using standard analysis techniques to ensure that high-quality films were deposited. The difference in the stoichiometric ratio and lattice mismatch between the passivation layer and substrate reduces the effect of surface passivation. Figure 7b and c show the Si-2*p* spectra of the EB-SiO and EB-SiO_2 passivation films, respectively, obtained through X-ray photoelectron spectroscopy (XPS). By calculating the peak areas of the Si and O elements, the content ratios of Si and O can be obtained. For the EB-SiO sample, the binding energy is 102.84 eV, which is located between the absorption peaks of the 2 and + 4 valence states. However, the binding energy corresponding to the strongest absorption peak of EB-SiO_2 is 103.66 eV. This corresponds to the main absorption peak of SiO_2, and no other peak appears from 99 eV (Si) to 103.6 eV (SiO_2). The atomic ratios of O to Si in EB-SiO and EB-SiO_2 are 1.140 and 1.97, respectively. As the oxygen content increases, the main absorption peak of Si shifts to the right, and the binding energy and valence of Si increases gradually.

The minority carrier lifetime of the passivation film is one of the main parameters used to characterize the quality of the SiO_x passive films. The results show that the minority carrier lifetime of the passivation film SiO_2 is 21.3 μs, which is higher than that of Ge-SiO. This means a lower defect density, higher short-range order, and better passivation effect. In addition, the high minority carrier lifetime can reduce the recombination rate of electron–hole pairs.

The passivation mechanism of different films was further analyzed based on the minority carrier lifetime and XPS measurements. Passivation of the sample surface reduces the surface recombination rate and affects the minority carrier lifetime [33]. The recombination of carriers is generated by the defect energy level (surface state) in the band gap. The suspended bond density of the sample surface is reduced by a combination of silicon oxide and dangling bonds, thus decreasing the density of the impurity energy level and the recombination center of minority carriers. EB-SiO_2 provides a surface with relatively fewer dangling bonds and then decreases the DOSs and surface recombination velocity, further increasing the minority carrier lifetime.

The characteristics of the SiO_x passive film affect the surface performance, and these characteristics depend largely on the sputtering deposition process parameters. The Ge surface between the electrical contacts must be passivated to minimize the surface-related leakage current. In addition, the intercontact surface must generate minimal dielectric noise. The surface leakage noise and passivant dielectric noise must remain low to achieve an acceptable signal-to-noise ratio.

Silicon oxides have been investigated as an alternative to H passivation for germanium detectors. The increase in the minority carrier lifetime near the interface leads to a decrease in the leakage current. Stable surface passivation is key to the application of Ge devices. The surface passivation layer should meet the requirements of a stable valence bond, high voltage, low dielectric constant, and high resistance layer. An effective surface passivation method can provide a surface with a smooth atomic arrangement and fewer dangling bonds and surface contaminants [34–36]. Controlling the surface chemistry and passivating Ge surfaces to achieve a consistently neutral intercontact surface is of paramount importance in the success of HPGe detector manufacturing processes and enhanced durability for long-term operation.

4 Conclusion

The performance of HPGe needs to be improved with long-term reliability and high resolution via surface passivation techniques. The interface quality of Ge is very important because it cannot form a stable oxide layer similar to silicon dioxide, thus affecting its chemical stability and electrical properties.

The band structures of Ge–H, Ge-NH_2, Ge-OH, and Ge-SiO_x termination systems were simulated using first-principles calculations. The band gap of Ge with different terminated atoms and groups was reduced to different degrees with Ge-OH and Ge-SiO_x of indirect band gaps and Ge–H and Ge-NH_2 of the direct band gap. The band gap of Ge–H was significantly larger than that of the Ge single crystal. The *s*-orbital of H interacted with the *p*-orbital of the outer Ge atoms, causing the DOS peak to move away from the band edge and reduce the DOS of the surface Ge atom near the Fermi level.

The DOS of the *s*-orbital of Ge-OH was significantly lower than that of the *p*-orbitals, indicating that the passivation effect of the OH group is slightly better than that of the H and NH_2 terminations. H, N, and O atoms can effectively reduce the DOS of the Ge-based system, and the passivation effect of O atoms performed well. Because of

the random mixing and bonding of Si and O atoms in the passivation layer of Ge, Ge-SiO_2 offers the best passivation effect by reducing the DOS intensity. This helps explore the application in HPGe detectors with ultralow surface leakage current.

The relationship between the preparation parameters and electronic characteristics of SiO and SiO_2 passive films was systematically studied. The different Si/O ratios have various defect state densities, and their conduction depends on the electron hopping in the local state near the Fermi level. The SiO_2 passivation film by electron beam evaporation has a higher resistivity and minority carrier lifetime. This confirms that SiO_2 reduces the recombination rate and eliminates the effect of surface recombination more effectively. This passivation technique, which can reduce the surface recombination of the outermost Ge atoms, provides superior resolution and reliability in HPGe and offers a critical application in the particle detection of HPGe detectors. The passivation effect and mechanism were discussed in terms of hopping conduction and surface defect density.

Acknowledgements The authors are very thankful for the valuable suggestions provided by Yang Tian and Yu-Lan Li from Department of Engineering Physics, Tsinghua University. Thanks are also given to the Open Fund of Key Laboratory of Particle Technology and Radiation Imaging (Ministry of Education) at Tsinghua University. We are grateful to all members of the Joint Laboratory of Beijing Normal University-Jinping Underground Laboratory.

Author contributions All authors contributed to the study conception and design. Simulation was preformed by Sha-sha Lv. Material preparation, data collection, and analysis were preformed by Sha-sha Lv, Yuan-Yuan Liu, Wei-You Tang, Xiu-Xia Li, and Li He. The first draft of the manuscript was written by Sha-sha Lv, and all authors commented on previous of the manuscript. All authors read and approved the final manuscript.

References

1. H. Jiang, L.P. Jia, Q. Yue, C.D.E.X. Collaboration et al., Limits on light weakly interacting massive particles from the first 102 8 kg×day data of the CDEX-10 experiment. Phys. Rev. Lett. **120**, 241301 (2018). https://doi.org/10.1103/PhysRevLett.120.241301
2. M. Agostini, I. Keshelashvili, J. Ahrens et al., GERDA collaboration, improved limit on neutrinoless double-β Decay of ^{76}Ge from GERDA Phase II. Phys. Rev. Lett. **120**, 132503 (2018). https://doi.org/10.1103/PhysRevLett.120.132503
3. C.E. Aalseth, N. Abgrall, E. Aguayo, Majorana Collaboration et al., A search for neutrinoless double-β decay in ^{76}Ge with the majorana demonstrator. Phys. Rev. Lett. **120**, 132502 (2018). https://doi.org/10.1103/PhysRevLett.120.132502
4. H. Jiang, Q. Yue, Y.L. Li et al., Measurement of the dead layer thickness in a p-type point contact germanium detector. Chinese Phys. C **40**, 096001 (2016). https://doi.org/10.1088/1674-1137/40/9/096001
5. N. Abgrall, E. Aguayo, F.T. Avignone et al., The majorana low-noise low-background front-end electronics. Phys. Proc. **61**, 654–657 (2015). https://doi.org/10.1016/j.phpro.2014.12.066
6. M. Agostini, A.M. Bakalyarov, M. Balata, G.E.R.D.A. collaboration et al., Upgrade for phase II of the GERDA experiment. Eur. Phys. J. C. **78**, 388 (2018). https://doi.org/10.1140/epjc/s10052-018-5812-2
7. R. Agnese, A.J. Anderson, M. Asai et al., CDMSlite: a search for low-mass WIMPs using voltage-assisted calorimetric ionization detection in the SuperCDMS experiment. Phys. Rev. Lett. **112**, 041302 (2014). https://doi.org/10.1103/PhysRevLett.112.041302
8. G. Ambrosi, Q. An, R. Asfandiyarov et al., Direct detection of a break in the teraelectronvolt cosmic-ray spectrum of electrons and positrons. Nature **552**, 63–66 (2017). https://doi.org/10.1038/nature24475
9. A. Benoit, L. Berge, J. Blumer et al., Sensitivity of the EDELWEISS WIMP search to spin-dependent interactions. Phys. Lett. B. **616**, 25–30 (2005). https://doi.org/10.1016/j.physletb.2005.04.052
10. E. Armengaud, Q. Arnaud, C. Augier et al., Performance of the EDELWEISS-III experiment for direct dark matter searches. J. Instrum. **12**, P08010 (2017). https://doi.org/10.1088/1748-0221/12/08/P08010
11. C.E. Aalseth, P.S. Barbeau, J. Colaresi et al., CoGeNT: A search for low-mass dark matter using p-type point contact germanium detectors. Phys. Rev. D **88**, 012002 (2013). https://doi.org/10.1103/PhysRevD.88.012002
12. W. Zhao, Q. Yue, K.J. Kang et al., First results on low-mass WIMPs from the CDEX-1 experiment at the China Jinping underground laboratory. Phys. Rev. D **88**, 052004 (2013). https://doi.org/10.1103/PhysRevD.88.052004
13. Q. Yue, W. Zhao, K.J. Kang et al., Limits on light weakly interacting massive particles from the CDEX-1 experiment with a p-type point-contact germanium detector at the China Jinping Underground Laboratory. Phys. Rev. D **90**, 091701 (2014). https://doi.org/10.1103/PhysRevD.90.091701
14. W. Zhao, Q. Yue, K.J. Kang et al., Search of low-mass WIMPs with a p-type point contact germanium detector in the CDEX-1 experiment. Phys. Rev. D **93**, 092003 (2016). https://doi.org/10.1103/PhysRevD.93.092003
15. Y.Y. Liu, J.P. Cheng, P. Pang et al., Developing cold-resistant high-adhesive electronic substrate for WIMPs detectors at CDEX. Chin. Phys. B **29**, 045203 (2020). https://doi.org/10.1088/1674-1056/ab718a
16. J.L. Ma, Q. Yue, S.T. Lin et al., Study on cosmogenic activation in germanium detectors for future tonne-scale CDEX experiment. Sci. China- Phys. Mech. Astronomy **62**, 011011 (2019). https://doi.org/10.1007/s11433-018-9215-0
17. K. Kato, H. Kondo, M. Sakashita et al., Formation processes of Ge_3N_4 films by radical nitridation and their electrical properties. Thin Solid Films **518**, S226–S230 (2010). https://doi.org/10.1016/j.tsf.2009.10.094
18. T. Maeda, T. Yasuda, M. Nishizawa et al., Pure germanium nitride formation by atomic nitrogen radicals for application to Ge metal-insulator-semiconductor structures. J. Appl. Phys. **100**, 014101 (2006). https://doi.org/10.1063/1.2206395
19. B.L. Yang, Q. Zhou, J. Zhang et al., Performances of different efficiency calibration methods of high-purity-germanium gamma-ray spectrometry in an inter-comparison exercise. Nucl. Sci. Tech. **30**, 37 (2019). https://doi.org/10.1007/s41365-019-0562-x
20. Y.L. Yan, W.X. Zhong, S.T. Lin et al., Study on cosmogenic radioactive production in germanium as a background for future rare event search experiments. Nucl. Sci. Tech. **31**, 55 (2020). https://doi.org/10.1007/s41365-020-00762-1
21. Y.L. Song, F.Q. Zhou, Y. Li et al., Methods for obtaining characteristic γ-ray net peak count from interlaced overlap peak in

HPGe γ-ray spectrometer system. Nucl. Sci. Tech. **30**, 11 (2019). https://doi.org/10.1007/s41365-018-0525-7
22. L. Merid, F. Giorgos, N. Michael, Modifying the band gap and optical properties of Germanium nanowires by surface termination. Appl. Surf. Sci. **396**, 1155–1163 (2017). https://doi.org/10.1016/j.apsusc.2016.11.104
23. P. Alfaro, A. Miranda, A.E. Ramos et al., Hydrogenated Ge nanocrystals: band gap evolution with increasing size. Braz. J. Phys. **36**, 375–378 (2006). https://doi.org/10.1590/S0103-97332006000300038
24. A.B. Greytak, L.J. Lauhon, M.S. Gudiksen et al., Growth and transport properties of complementary germanium nanowire field-effect transistors. Appl. Phys. Lett. **84**, 4176 (2004). https://doi.org/10.1063/1.1755846
25. Y. Wu, P. Yang, Germanium nanowire growth via simple vapor transport. Chem. Mater. **12**(3), 605–607 (2000). https://doi.org/10.1021/cm9907514
26. S. Carturan, G. Maggioni, S.J. Rezvani et al., Wet chemical treatments of high purity Ge crystals for γ-ray detectors: Surface structure, passivation capabilities and air stability. Mater. Chem. Phys. **161**, 116–122 (2015). https://doi.org/10.1016/j.matchemphys.2015.05.022
27. G.P. Collins, S. Barth. Fleming et al., Alkane and alkanethiol passivation of halogenated Ge nanowires. Chem. Mater. **22**(23), 6370–6377 (2010). https://doi.org/10.1021/cm1023986
28. K. Vetter, Recent developments in the fabrication and operation of germanium detectors. Annu. Rev. Nucl. Part. Sci. **57**, 363–404 (2007). https://doi.org/10.1146/annurev.nucl.56.080805.140525
29. A.P. Alivisatos, Semiconductor clusters, nanocrystals, and quantum dots. Science **271**, 933–937 (1996). https://doi.org/10.1126/science.271.5251.933
30. M. Legesse, G. Fagas, M. Nolan, Modifying the band gap and optical properties of Germanium nanowires by surface termination. Appl. Surf. Sci. **396**, 1155–1163 (2017). https://doi.org/10.1016/j.apsusc.2016.11.104
31. C. Fleischmann, K. Schouteden, M. Müller et al., Impact of ammonium sulfide solution on electronic properties and ambient stability of germanium surfaces: towards Ge-based microelectronic devices. J. Mater. Chem. C **1**, 4105–4113 (2013). https://doi.org/10.1039/C3TC30424H
32 Y.B. Gurov, V.S. Karpukhin, S.V. Rozov et al., Passivation of HPGe detectors. Instrum. Exp. Tech. **52**, 137–140 (2009). https://doi.org/10.1134/S0020441209010230
33. M. Jing, M. Ni, W. Song et al., Anisotropic and passivation-dependent quantum confinement effects in germanium nanowires: a comparison with silicon nanowires. J. Phys. Chem. B **110**(37), 18332–18337 (2006). https://doi.org/10.1021/jp063518j
34. D. Dass, Effects of surface passivation by hydrogen on the structural and electronic properties of a germanium nanowire: A sp3 tight binding study. Appl. Surf. Sci. **488**, 404–417 (2019). https://doi.org/10.1016/j.apsusc.2019.05.230
35. T. Comellato, M. Agostini, S. Schönert, Charge-carrier collective motion in germanium detectors for ββ-decay searches. Eur. Phys. J. C **81**, 76 (2021). https://doi.org/10.1140/epjc/s10052-021-08889-0
36. T. Maeda, T. Yasuda, M. Nishizawa et al., Pure germanium nitride formation by atomic nitrogen radicals for application to Ge metal-insulator-semiconductor structures. J. Appl. Phys. **100**, 014101 (2006). https://doi.org/10.1063/1.2206395